Dalton Transactions

ROYAL SOCIETY OF CHEMISTRY

PAPER

View Article Online
View Journal | View Issue

Cite this: *Dalton Trans.*, 2024, **53**, 14108

$Mg_{2-x}Ca_xAl$ layered double hydroxide-derived mixed metal oxide porous hexagonal nanoplatelets for CO_2 sorption†

Bhojaraj,[a] C. Nethravathi *[a,b] and Michael Rajamathi *[a]

Received 6th June 2024,
Accepted 17th July 2024

DOI: 10.1039/d4dt01647e

rsc.li/dalton

Porous hexagonal nanoplatelets of mixed metal oxide (MMO) derived from the calcination of MgAl layered double hydroxide exhibits a CO_2 sorption capacity of 1.99 mmol g^{-1} at 30 °C, with a retention of 87% sorption capacity over 10 carbonation–decarbonation cycles and a CO_2 sorption capacity of 1 mmol g^{-1} at 200 °C with a 40% increase in capacity over 10 cycles. The high sorption capacity is attributed to the porous nanoplatelet structure of the MMO with a BET surface area of 115 m^2 g^{-1}, which enables increased CO_2 diffusion. Upon partially replacing magnesium with calcium (33, 50 and 66 mol%), the CO_2 sorption capacity of the MMO increases with an increase in temperature. MMO derived from LDH, in which 66% of magnesium is replaced by calcium (MgCaAl-66), delivers CO_2 sorption capacities of 1.38, 1.31, 2.50, 4.85 and 7.75 mmol g^{-1} at 200, 300, 350, 400 and 600 °C, respectively, which is significant for application in the sorption-enhanced water gas shift (SEWGS) process. MgCaAl-66 MMO exhibits a sorption capacity of 1 mmol g^{-1}, which is stable over 10 cycles at 200 °C, and a sorption capacity of 3.68 mmol g^{-1} at 400 °C with 85% capture efficiency retention over 10 cycles. While the incorporation of Ca^{2+} serves multiple purposes such as increasing basic defect sorption sites and improving stability to repress the sintering-induced limitation of MMO over sorption cycles, the porous nanoplatelets act as individual sorbent units resisting volume changes through carbonation–decarbonation cycles.

1. Introduction

Carbon dioxide capture using solid sorbents *via* weak physical (adsorption) or strong chemical (acid–base) interactions is a viable option to handle anthropogenic CO_2 emissions.[1–4] Solid sorbents yield high sorption efficiency and durability owing to the tuneable wide range of sorption conditions (temperature/CO_2 concentration/chemical compositions), facile regeneration, and cycling stability.[1–4] At low temperatures (< 200 °C), amines[5,6] chemisorb CO_2, while carbon,[7] silica,[8] zeolite/MOFs/COFs,[9] and clays[10] exhibit surface area controlled weak physisorption. Intermediate temperature (200–400 °C) sorbents mineralize CO_2 through adsorption within the morphological pores of metal oxides such as MgO[11] and layered double hydroxide (LDH)-derived mixed metal oxides (MMOs).[1,2] Basic CaO-based materials sorb CO_2 at high temperatures (>400 °C).[12] The other promising CO_2 capture strategy is the sorption-enhanced water–gas shift process (SEWGS), a pre-combustion technology, wherein the primary fuel is first combusted in the presence of steam/oxygen, yielding syngas (CO and H_2O), which is converted to CO_2 and H_2 by means of a water gas shift reaction at 200–450 °C and under high pressures.[1–4] At this point, sorption of CO_2 by a sorbent shifts the reaction equilibrium, enhancing the conversion percentage.

MMOs with a large surface area, abundant basic sites, rapid sorption/desorption kinetics, structural/thermal stability, moisture tolerance, high affinity and selectivity for CO_2 mineralization are potential solid sorbents for acidic CO_2 sorption at 200–450 °C.[1–4]

LDHs are lamellar anionic clays[13–15] comprising tuneable positively charged metal hydroxide layers and charge balancing anions in the interlayer, which can be exchanged[16,17] for a variety of anions, including inorganic anions,[18–20] aliphatic/aromatic acids[21–23] and biomolecules.[24,25] The nominal composition of LDH is $[M^{II}_{(1-x)}M^{III}_x(OH)_2]A^{n-}_{x/n}{\cdot}mH_2O$, {$M^{II}$ = Mg, Co, Ni, Cu, Zn or Ca; M^{III} = Al, Cr, Fe or Ga; A^{n-} = anion with a valency n; $x = [M^{III}]/([M^{II}] + [M^{III}])$, ranging from 0.25 and 0.33}.[13–15] Thermal decomposition of LDH yields MMO. Depending on the composition of the LDH and the decomposition temperature, the product of decomposition is a defect

[a]*Materials Research Group, St Joseph's University, 36, Lalbagh Road, Bangalore, 560027, India. E-mail: michael.rajamathi@sju.edu.in*
[b]*Department of Chemistry, Mount Carmel College, Bangalore 560052, India. E-mail: nethravathic@gmail.com*

†Electronic supplementary information (ESI) available. See DOI: https://doi.org/10.1039/d4dt01647e

oxide with significant trivalent cation content or a stable spinel. Usually, the defect oxide is reconstructed into LDH in the presence of anions.[13–15] The widely available mineral hydrotalcite, $[Mg_3Al(OH)_8]_2CO_3{\cdot}xH_2O$, and its calcined product are potential sorbents employed in environmental amelioration.[21] Studies indicate that CO_2 is sorbed as bicarbonate on weakly basic surface hydroxyl groups of MMO or as carbonates on surface oxygen atoms with different coordination degrees. While unidentate irreversible carbonate species are formed on oxygen ions with the lowest coordination number (O^{2-}, strong base sites), reversible chelating and bridging bidentate carbonates require an adjacent cationic site (M^+–O^{2-} pairs, moderate base sites).[26]

Low CO_2 sorption capacity is the major limitation of MMO as a sorbent. The surface area, basicity of active sorption sites and mechanical stability influence the CO_2 chemisorption capacity of MMO. To address these issues, various strategies[1–4] have been employed such as (i) morphology-controlled synthesis, (ii) hybridization of LDH with graphite oxide (GO), (iii) varying M^{2+}–M^{3+} composition, (iv) varying the M^{2+}/M^{3+} ratio, (v) changing interlayer anion, and (vi) impregnation with an alkali metal cation. Synthesis of LDH at different pH values in the presence of structure-directing agents yields hierarchical structures with increased surface area.[27] The Mg_3Al-CO_3 LDH with different morphologies, sand rose (114 $m^2\ g^{-1}$) and spherical nanoparticles (103 $m^2\ g^{-1}$) (but similar surface area), exhibit comparable sorption capacity (200 °C) of 0.53 and 0.58 mmol g^{-1}, respectively.[28] The CO_2 sorption performance of the 3D nanoflower-like structure of the Mg_2Al-CO_3 LDH-derived MMO (365 $m^2\ g^{-1}$) is 0.9 mmol g^{-1} at 200 °C.[29] Exfoliation of LDH yields 2D hydroxide layers, offering a large surface area for CO_2 sorption. MMO derived from the exfoliated 2-D Zn_3Al-NO_3 LDH (surface area = 455 $m^2\ g^{-1}$) delivers a sorption capacity of 2.93 mmol g^{-1} at 200 °C, while the MMO derived from the bulk 3D Zn_3Al-NO_3 LDH (surface area = 49 $m^2\ g^{-1}$) offers a capacity of 1.1 mmol g^{-1}.[30] $Mg_{0.7}Al_{0.3}(OH)_2{\cdot}0.036(W_7O_{39}){\cdot}0.08NO_3$ with a surface area of 136 $m^2\ g^{-1}$ prepared by the reassembly of exfoliated 2D LDH layers in the presence of polyoxometalate shows a sorption capacity of 0.74 mmol g^{-1} at 25 °C in comparison to 0.08 mmol g^{-1} shown by $Mg_{0.7}Al_{0.3}$-NO_3 LDH (surface area = 25 $m^2\ g^{-1}$).[31] The synergy between the components affects the properties of the composite. Hybridization of the two-layered components, LDH and graphite oxide with geometric and charge compatibility, improves the active sorbent morphology, dispersion, and thermal stability, leading to an enhancement of the CO_2 uptake capacity to 0.45 mmol g^{-1} at 300 °C (0.2 bar).[32] The combination of divalent (Mg^{2+}, Ca^{2+}, Co^{2+}, Ni^{2+}) and trivalent cations (Al^{3+}, Ga^{3+}, Fe^{3+}, Mn^{3+}) not only directs the calcination temperature of the LDH to form the quasi-amorphous MMO, but also determines the stability of the MMO phase, thus affecting the CO_2 sorption capacity at the desired sorption temperature. Mg_3Al LDH calcined at 400/500 °C sorbs 0.410/0.387 mmol g^{-1} at 200 °C, whereas Mg_3Mn LDH calcined at 250/400 °C sorbs 0.422/0.089 mmol g^{-1} at 200 °C respectively.[33] In the case of Mg_3Mn LDH, the formation of Mg_2MnO_4 in the presence of MgO at 400 °C reduces the sorption capacity. Conversely, only periclase MgO is formed in the case of Mg_3Al LDH. The M^{2+}/M^{3+} ratio influences the basicity of the sorption sites. In the case of commercial MgAl LDH (SASOL) with a Mg : Al ratio of 2 : 1, 1 : 2, and 3 : 1 calcined at 450 °C, the highest sorption capacity (0.32 mmol g^{-1}) was observed in the case of the 2 : 1 ratio at 400 °C.[34] While the Mg–O sites are believed to be active CO_2 sorbent sites, Al^{3+} induces the defects and activates the Mg–O sites. Tertiary oxides formed upon the addition of M^{2+}/M^{3+} cations to LDH have been shown to deliver enhanced sorption capacity that is controlled by the density and basicity of the active sorption sites. $Mg_2(Al_{0.9}Ga_{0.1})(OH)_6(CO_3)_{0.5}$ calcined at 400 °C exhibits 1.15 mmol g^{-1} sorption capacity at 300 °C.[35] $Mg_2CaAl(OH)_8(CO_3)_{0.5}$ and $Ca_{1.5}Co_{1.5}Al(OH)_8(CO_3)_{0.5}$ calcined at 550 °C exhibit sorption capacities of 1.28 and 1.39 mmol g^{-1}, respectively, at 350 °C.[36] The Mg_3Al-CO_3 LDH with the highest basic site density (692 mmol g^{-1}) delivers the maximum CO_2 sorption capacity (0.53 mmol g^{-1}) in comparison to Mg_3Al LDH with $NO_3^-/SO_4^{2-}/Fe(CN_6)^{4-}/Cl^-/ClO_4^-$ in the interlayer.[37] Mg_3Al–stearate exhibits higher sorption capacity (1.25 mmol g^{-1}) than Mg_3Al-CO_3 (0.5 mmol g^{-1}).[38] The repressed memory effect of calcined Mg_3Al–stearate was believed to result in a stable quasi-amorphous structure with enriched surface basicity. Modification of LDH with optimum amounts of alkali metal cations (K, Na, Cs) causes an increase in the concentration of defects (low coordination oxygen sites) and surface basicity, thus improving the sorption capacity. However, the higher loading of alkali metal cations leads to clogged pores and poor sorption. Commercial Mg_3Al-CO_3 LDH doped with 20% K_2CO_3 calcined at 450 °C exhibits a sorption capacity (at 400 °C) of 0.83 mmol g^{-1} in comparison to 0.22 mmol g^{-1} in the case of undoped LDH.[34]

It is important to design materials that incorporate a high surface area, optimum basicity[39] and stability (structural/morphological)[40] to maximize the CO_2 sorption across a wide temperature range. This work explores the CO_2 sorption behaviour of calcium ion-incorporated hexagonal platelets of MgAl-CO_3 LDH in terms of the concentration of calcium ions, calcination temperature of the LDH, and the CO_2 sorption temperature. Nanoscale hexagonal platelet morphology and incorporation of Ca^{2+} serve multiple purposes. They induce and increase the basic defect sorption sites, and improve the stability to repress the sintering-induced limitation of MMO over sorption cycles. Porous hexagonal nanoplatelets act as individual sorbent units that resist volume changes through carbonation–decarbonation cycles.

2. Experimental section

2.1 Preparation of MgCaAl-carbonate LDH and mixed metal oxide

$Mg_2Al(OH)_6(CO_3)0.5{\cdot}mH_2O$ (MgCaAl-0) and calcium-modified LDH were prepared by urea hydrolysis method, as reported in the literature.[19] An aqueous solution (50 mL) containing metal

salts and urea was subjected to a hydrothermal reaction at 180 °C for 2 h in a Teflon-lined autoclave. The product was washed with water and dried in an air oven at 65 °C. MMO was prepared by heating the LDH in air at the desired temperature for 3 h, followed by cooling in a desiccator. The masses of salts used in the preparation of a specific LDH composition are shown in Table 1.

2.2. CO_2 sorption

The cyclic CO_2 capture capacities of porous MMO hexagonal nanoplates were evaluated in a thermogravimetric analyzer (PerkinElmer STA 6000) at ambient pressure. All heating and cooling cycles were carried out at a ramping rate of 10 °C min^{-1}. The sample (~3 mg) was loaded in a 250 μL alumina crucible and heated to 800 °C under nitrogen flow (20 mL min^{-1}). After calcination (15 min) at 800 °C, the sample was cooled down to the desired sorption temperature (30, 100, 300, 350, 400 and 600 °C) and then equilibrated with CO_2 (20 vol% CO_2 in N_2, 20 mL min^{-1}) for 30 min. Following carbonation, the sorbent was regenerated by increasing the temperature to 700 °C in a N_2 atmosphere and isothermally heated at the same temperature for 5 min. The carbonation and decarbonation steps were repeated for the desired number of cycles. Saturation curves of CO_2 sorption were obtained at 30 °C and 600 °C over a period of three hours. The change in the mass of the sorbent was continuously monitored and recorded. The capture capacity is reported based on the total mass of the sorbent.

2.3. Characterisation

All solid products were characterized by powder X-ray diffraction (XRD) using a PANalytical X'pert PRO diffractometer (Cu Kα, λ = 1.5418 Å) fitted with a secondary graphite monochromator. Diffraction patterns were recorded from 5° to 70°, with a step size of 0.020° and time per step of 2.4 s, using slit widths of $\frac{1}{2}$ and 1 mm. The powder samples were loaded on a quartz sample holder to record the XRD data. Scanning electron microscopy (SEM) images were recorded using a Zeiss, Ultra 55 field emission scanning electron microscope. Metal ion (Mg^{2+}, Ca^{2+} and Al^{3+}) contents in the MMO were determined by atomic absorption spectrometry (Varion AA240 spectrometer). Nitrogen sorption analysis was performed at liquid nitrogen temperature using a BEL SORP mini-X instrument equipped with a BEL PREP VAC III degasser. The surface area of the material was determined by employing the Brunauer–Emmett–Teller (BET) equation.

Table 1 Reactant composition used in the synthesis of LDH samples

	Mass (g)			
Sample	$Mg(NO_3)_2 \cdot 6H_2O$	$Al(NO_3)_3 \cdot 9H_2O$	$Ca(NO_3)_2 \cdot 4H_2O$	Urea
MgCaAl-0	3.06	2.25	—	9.6
MgCaAl-33	2.05		0.94	
MgCaAl-50	1.54		1.41	
MgCaAl-66	1.02		1.88	

3. Results and discussion

The composition of the MgAl LDH (MgCaAl-0) was determined as reported in our earlier work,[19] and the nominal formula of this LDH is $Mg_2Al(OH)_6(CO_3)_{0.5} \cdot 1.8H_2O$. The XRD pattern of this LDH (Fig. 1a) shows a basal spacing of 7.5 Å and Bragg reflections corresponding to the $3R_1$ polytype.[41] A similar LDH phase is observed in the cases of samples prepared by replacing magnesium ions with 33, 50, and 66 atomic percent of calcium ions, except for the additional peaks due to gibbsite $Al(OH)_3$ (JCPDS 76-1782), whose intensity increases with Ca^{2+} content. Sharp peaks indicate that the LDH is crystalline and ordered. The compositions of the calcium ion-modified LDH are summarized in Table 2.

The XRD patterns of MgCaAl-0 calcined at various temperatures are shown in Fig. 2. On calcination at 300 °C, the lamellar phase of LDH is largely retained, although the structure is highly disordered due to the loss of the interlayer water, which confers ordering through hydrogen bonding. Broad peaks (Fig. 2c and d) corresponding to rock salt-type periclase MgO[42] is observed on calcination of CO_3-LDH at 600 °C and 800 °C. However, it has been shown by ^{27}Al MAS-NMR studies that the calcined (600 °C) hydrotalcite is an Al-modified MgO phase with Al atoms in tetrahedral sites.[43–46] Through XRD simulation studies and analysis of the solid obtained on leaching out the amphoteric Al from the calcined product, it has been suggested that the MMO is the Al-modified MgO with the spinel-type MgAl oxide present primarily on the surface of MgO.[45]

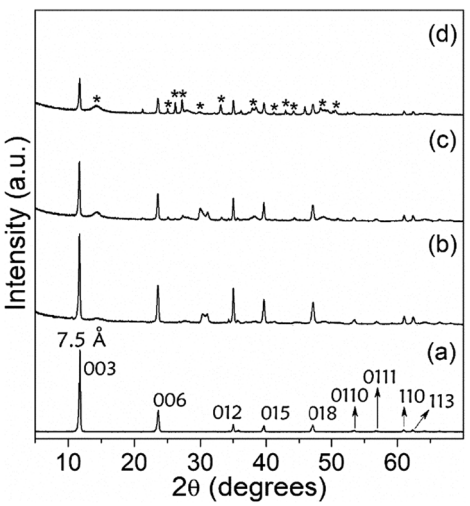

Fig. 1 XRD patterns of the as-prepared $Mg_{2-x}Ca_xAl\text{-}CO_3$-layered double hydroxide hexagonal nanoplatelets with 0% (a), 33% (b), 50% (c), and 66% (d) of Mg replaced with Ca. Peaks marked as * are from the Al $(OH)_3$ (gibbsite) phase.

Table 2 Composition analysis of the $Mg_{2-x}Ca_xAl\text{-}CO_3$ layered double hydroxide hexagonal nanoplatelets

	Mole ratio				
LDH	Mg	Ca	Al	[Ca] × 100/([Ca] + [Mg])	Nominal formula
MgCaAl-0	1.96	0	1.00	0	$Mg_2Al(OH)_6(CO_3)_{0.5}\cdot 1.8H_2O$
MgCaAl-33	1.32	0.71	1.00	34.9	$Mg_{1.3}Ca_{0.7}Al(OH)_6(CO_3)_{0.5}\cdot kH_2O$
MgCaAl-50	1.01	0.98	1.00	49.2	$MgCaAl(OH)_6(CO_3)_{0.5}\cdot mH_2O$
MgCaAl-66	0.72	1.26	1.00	63.6	$Mg_{0.7}Ca_{1.3}Al(OH)_6(CO_3)_{0.5}\cdot nH_2O$

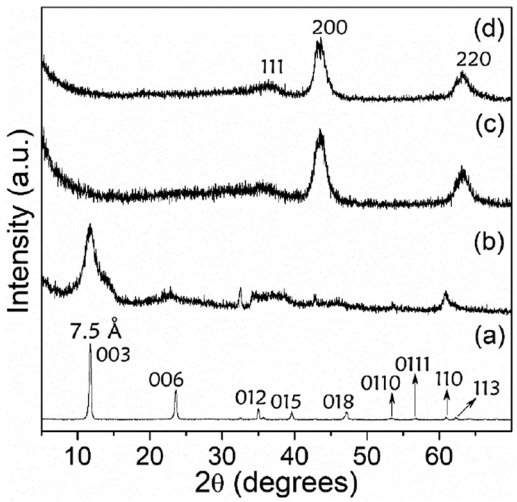

Fig. 2 XRD patterns of the as-prepared MgCaAl-0 LDH (a); and its calcination products at 300 °C (b), 600 °C (c), and 800 °C (d).

Effects of the BET surface area and calcination temperature of MgCaAl-0 on the CO_2 sorption capacity are summarized in Table 3. MMO obtained at 800 °C exhibits the highest sorption capacity (at 30 °C) compared to the 600 °C heated sample with a higher surface area (Table 3). This is possible because as the calcination temperature increases, more Al^{3+} ions substitute the Mg^{2+} ions in the periclase MgO lattice. Thus, each Al^{3+} substitution induces two active Mg–O species due to the adjacent unsaturated oxide ions.[47] The 800 °C calcined sample exhibits competitive sorption capacities (Table 4) of 1.45, 1.06 and 0.61 mmol g^{-1} at 30, 200 and 400 °C, respectively. These observations directed the sorption measurements to be carried out at SEWGS operating temperatures and exploration of the possibility to enhance the sorption capacity by modification of the LDH lattice. Further sorption measurements were carried out using samples calcined at 800 °C.

Table 3 Effect of calcination temperature on the CO_2 sorption capacity of MgCaAl-0 LDH at a sorption temperature of 30 °C

LDH	Calcination temperature (°C)	BET surface area (m^2 g^{-1})	CO_2 sorption capacity at 30 °C (mmol g^{-1})
MgCaAl-0	As-prepared	26.26	—
	300	35.05	0.39
	600	192.32	1.32
	800	115.18	1.99

MgAl-CO_3 LDH was prepared hydrothermally in the presence of various amounts of Ca^{2+} ions, as indicated in Table 1. MgCaAl-CO_3 LDH were prepared by replacing Mg^{2+} with 33, 50 and 66 mol% of Ca^{2+} ions. Calcination of MgCaAl-CO_3 LDH at 800 °C yields CaO dispersed in periclase MgO matrix (Fig. 3b–d). This is as expected since the Ca^{2+} ions with larger ionic radii are not expected to be incorporated in the periclase MMO lattice. The crystallite size of CaO increases with the Ca^{2+} content. The SEM images (Fig. 4) of the calcined (800 °C) MgCaAl LDH exhibit porous hexagonal nanoplatelets of ~1.5 μm lateral size and ~100 nm thickness in the cases of MgCaAl-0, 33, 50. Fused platelets of ~5 μm lateral size and ~100 nm thickness are observed in the case of MgCaAl-66. EDAX elemental analysis (Fig. 5) indicates the uniform distribution of Mg, Al and Ca in all of the calcined samples. In light of the observed morphology of the sorbent, the process involved in the CO_2 sorption is schematically represented in Fig. 6.

The CO_2 sorption responses of calcined (800 °C) MgCaAl-CO_3 LDH at different sorption temperatures are summarized in Table 4. As expected of a MgO based sorbent, the CO_2 sorption capacity of the MMO derived from MgCaAl-0 LDH decreases with the increase in the sorption temperature. At 200 °C, which is the lower end of the SEWGS operating temp-

Table 4 Effect of calcium content on the CO_2 sorption capacity of MgCaAl LDH calcined at 800 °C

		CO_2 sorption capacity (mmol g^{-1})					
LDH	BET surface area (m^2 g^{-1})	30 °C	200 °C	300 °C	350 °C	400 °C	600 °C
MgCaAl-0	113.52	1.45	1.06	0.60	0.54	0.61	0.36
MgCaAl-33	73.79	0.86	0.91	0.96	1.87	3.09	5.07
MgCaAl-50	99.68	0.86	0.97	1.15	2.39	4.55	6.25
MgCaAl-66	78.92	0.80	1.38	1.31	2.50	4.85	7.75

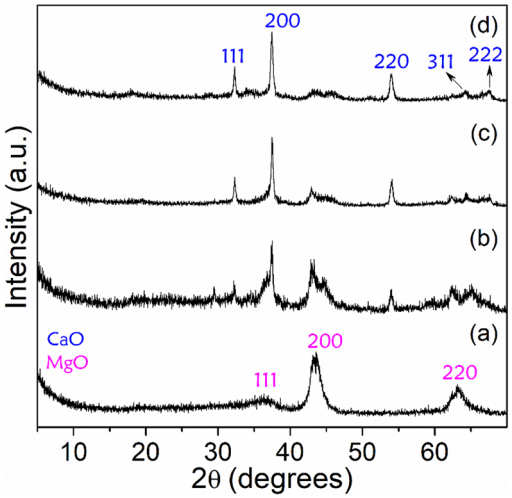

Fig. 3 XRD patterns of MgCaAl-0 LDH (a), MgCaAl-33 LDH (b), MgCaAl-50 LDH (c), and MgCaAl-66 LDH (d) calcined at 800 °C.

erature range (200–400 °C), this MMO offers an adequate, but non-competitive, CO_2 sorption capacity of 1.06 mmol g^{-1}. In contrast, the sorption capacity of all of the calcium modified MMO increases with sorption temperature and the maximum capacity is observed at 600 °C. These MMO exhibit excellent sorption capacities in the higher range of the SEWGS operating temperatures, rendering them as potential candidates for SEWGS promotion.

The carbonation profiles of the CO_2 sorption of porous MMO derived upon calcination of MgCaAl LDH with respect to time at two different sorption temperatures are shown in Fig. 7. In the case of sorption at 30 °C, the carbonation kinetics is fast at the onset of CO_2 uptake. This is followed by a slower sorption, leading to saturation and attaining equilibrium after ~2 h. This suggests that the initial chemisorption is followed by physisorption. In contrast, in the case of sorption at 600 °C, the sorption is fast and the equilibrium is reached within a few minutes. This indicates that the CO_2 uptake is due to chemisorption only.

The CO_2 affinity of the oxide sorbent and the available active sites determine the capture capacity.[36] The as-prepared LDH samples do not exhibit CO_2 sorption capacity. Calcination of LDH at an optimum temperature causes a loss of interlayer water, dehydroxylation and deanation, resulting in the formation of a porous mixed metal oxide with a poorly defined 3D network suitable for CO_2 sorption.[42,47] Calcination has dual functions; namely, the formation of pores (thus increasing the surface area and pore volume), and the induction of active sites to aid CO_2 sorption.[47,48] On calcination of LDH (>400 °C), Al^{3+} migrates into the periclase MgO lattice and substitutes Mg^{2+}, causing unsaturated adjacent oxygen anions and resulting in active Mg–O sites, but this simultaneously decreases the available surface Mg^{2+}.[47–49] Sorption of CO_2 on MMO takes place by a combination of both physisorption and chemisorption.[29,48–50] While CO_2 is chemisorbed

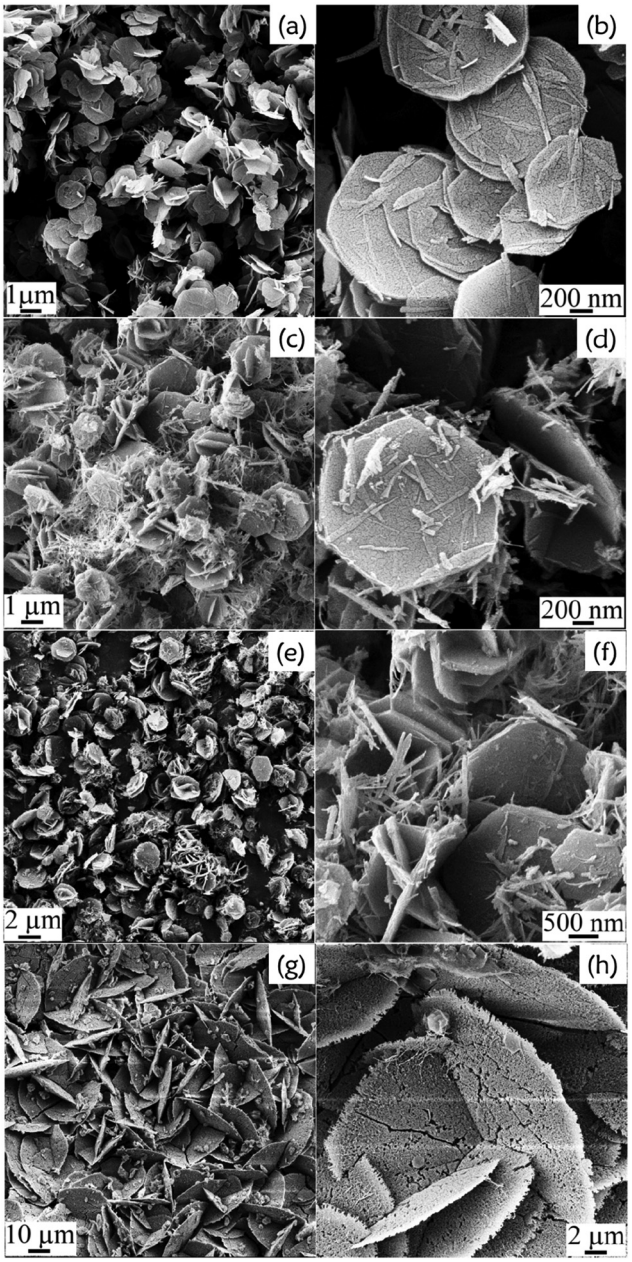

Fig. 4 SEM images of calcined (800 °C) LDH hexagonal nanoplatelets MgCaAl-0 (a and b); MgCaAl-33 (c and d); MgCaAl-50, (e and f); and MgCaAl-66 (g and h).

as a monolayer, the subsequent multilayer deposition controlled by pore size and volume is physisorptive and gradually loses the binding ability.[48–50] Calcined MgCaAl-0 delivers a sorption capacity of 1.45 mmol g^{-1} at 30 °C (Table 4 and Fig. 8A), which is largely attributed to the chemisorption of CO_2 and available moisture, as MMO is reconstructed back to the parent LDH by memory effect, as indicated by the XRD pattern of the sample after sorption (Fig. 8Ba). The sorption capacity decreases to 1.06 and 0.60 mmol g^{-1} at 200 °C and 300 °C, respectively, as the high surface area, pore volume and decreased availability of the surface Mg^{2+} favours physisorp-

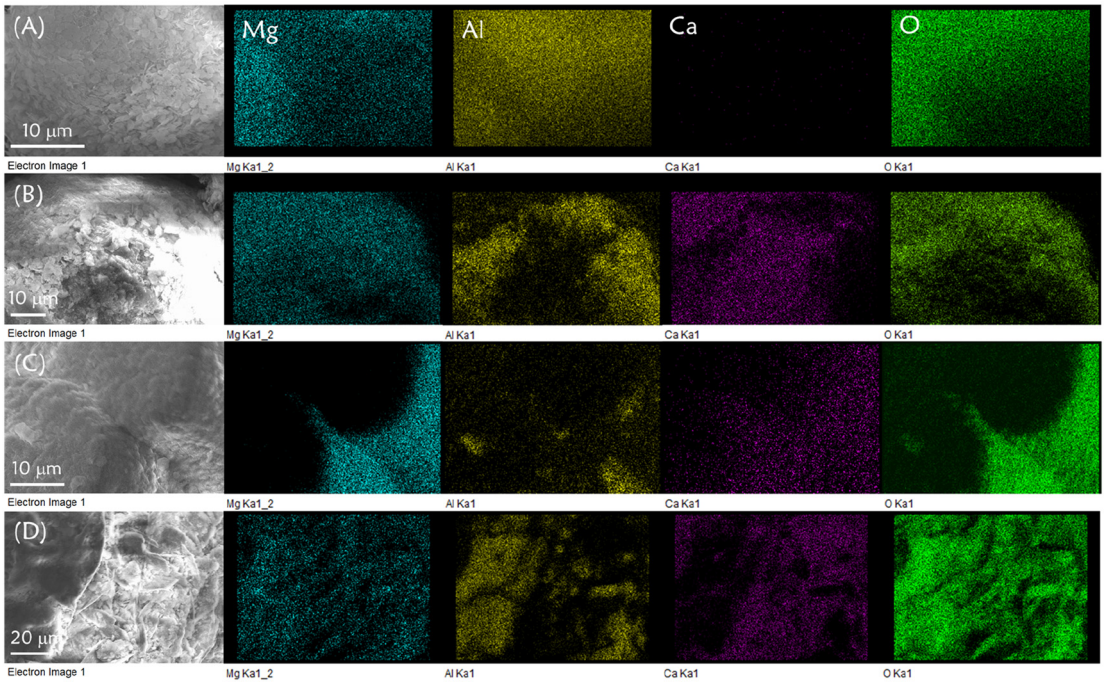

Fig. 5 SEM image and EDAX elemental mapping of magnesium, aluminium, calcium, and oxygen of calcined (800 °C) LDH hexagonal nanoplatelets: MgCaAl-0 (A); MgCaAl-33 (B); MgCaAl-50 (C); MgCaAl-66 (D).

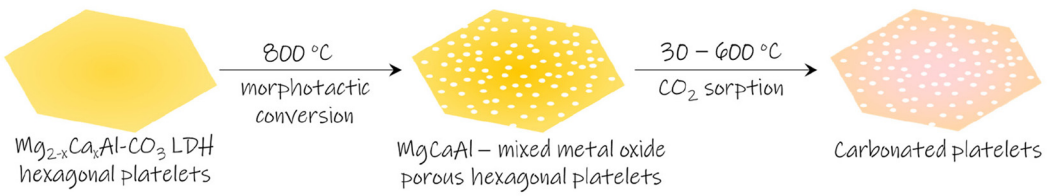

Fig. 6 Schematic representation of the stages involved in capturing CO_2 by LDH-derived MMO hexagonal platelets.

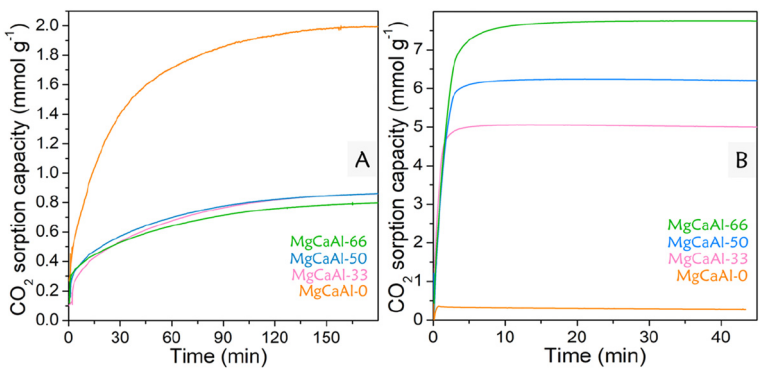

Fig. 7 Carbonation profiles at 30 °C (A) and 600 °C (B) of the CO_2 sorption of MgCaAl LDH calcined at 800 °C.

tion over chemisorption at higher sorption temperatures.[47–49] In addition, reconstruction of LDH is not possible at these temperatures. These observations are further corroborated by the XRD pattern of the sorbed sample (Fig. 8Bb), which is indexed to periclase MgO with no trace of $MgCO_3$ or LDH formation. Carbonation cycles (Fig. 8A) of the calcined porous MgCaAl-0 were carried out using thermogravimetric analysis (TGA) at atmospheric pressure under 20% CO_2 at 30 °C and 200 °C, and the decarbonation cycles were performed under 100% N_2 at 700 °C. The CO_2 capture cycles (Fig. 8A) display

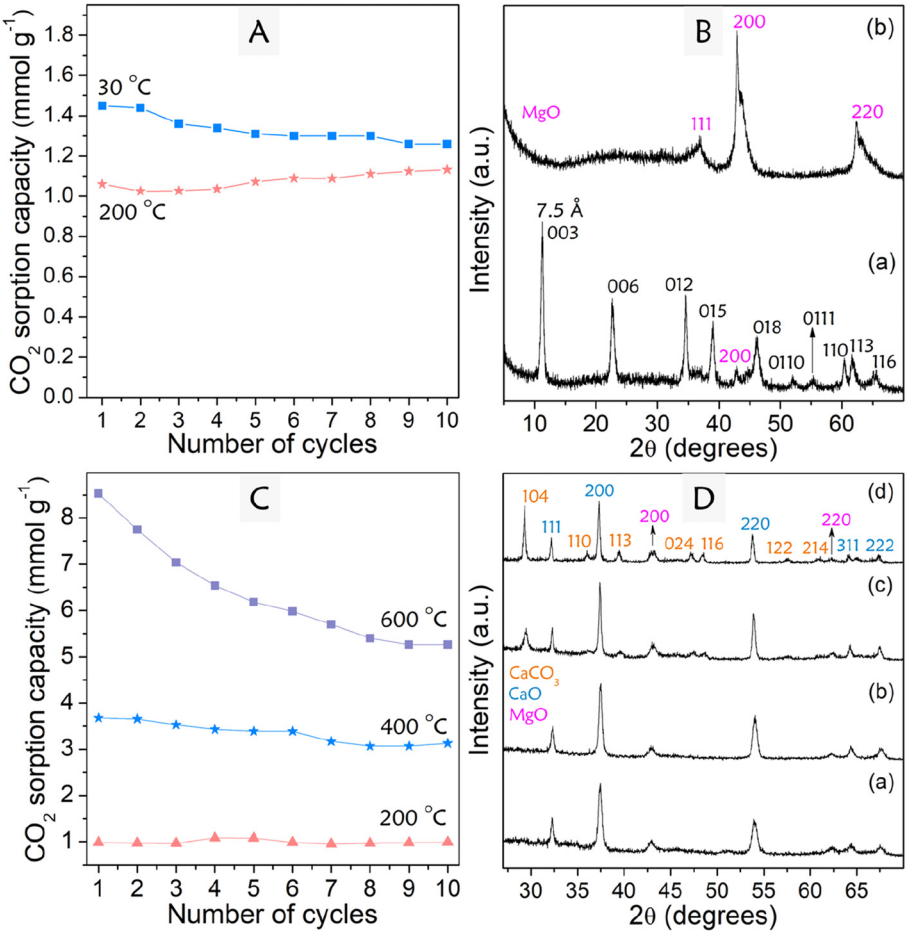

Fig. 8 CO_2 capture capacity over 10 carbonation–decarbonation cycles of MgCaAl-0 (A) and MgCaAl-66 (C) at different sorption temperatures. XRD patterns of MgCaAl-0 LDH (B) after sorption at 30 °C (a) and 200 °C (b); MgCaAl-66 LDH (D) after sorption at 30 °C (a), 200 °C (b), 400 °C (c) and 600 °C (d).

improved capture capacities and cycling stabilities in comparison to literature reports. At 30 °C, although the capture capacity steadily decreases with cycling, its capture efficiency retention (87%) is relatively high. The capture capacity at 200 °C steadily increases with cycling. This is possibly due to the increased diffusion of CO_2 on cycling.

In the case of the calcined MgCaAl-33, MgCaAl-50 and MgCaAl-66 samples, the sorption capacity increases with an increase in the temperature (Table 4). However, in the temperature range of 30–200 °C, the capacity is less compared to that of MgCaAl-0 (Table 4). Formation of stable CaO (Fig. 3b–d) in these samples hinders the chemisorption and reconstruction of MMO to the LDH phase, indicating that the CO_2 uptake largely occurs through physisorption at low temperatures.[36,47–49] The calcium-modified samples exhibit enhanced CO_2 sorption capacity in the SEWGS operating temperature range (200–400 °C) in comparison to related materials in the literature.[1–4] Sorption at higher temperatures (400 and 600 °C) is due to a combination of both physisorption and chemisorption, as indicated by the CaO, MgO and $CaCO_3$ peaks in the XRD patterns (Fig. 8Dc and d) of the sorbed samples of porous calcined MgCaAl-66. The improved performance of the calcined, Ca^{2+}-incorporated LDH is due to the following reasons: (i) the basic CaO is expected to increase the active MgO sites through its interaction with Al^{3+} in the periclase lattice.[36,47–49] (ii) The evenly dispersed CaO crystallites repress the sintering of the periclase particles, leading to an improved mechanical stability of the sorbent during the carbonation–decarbonation cycles. Porous calcined MgCaAl-66 delivers a stable sorption capacity (Fig. 8C) of 1 mmol g^{-1} over 10 cycles at 200 °C and a sorption capacity of 3.68 mmol g^{-1} at 400 °C with 85% capture efficiency retention after 10 cycles. The sorption capacity at 600 °C decreases rapidly with a 62% capture efficiency retention at the end of 10 cycles. This could be due to the hindered CO_2 diffusion through the $CaCO_3$ layers formed during sorption, which makes the unreacted CaO and the porous network inaccessible to CO_2.[36]

The cycling performance (Fig. 9) of the porous calcined MgCaAl LDH compositions was also probed at 350 °C, SEWGS operating temperature. All of the calcium modified sorbents exhibited enhanced sorption capacity and stability. Over 10 sorption–desorption cycles, MgCaAl-33 delivers 24% loss,

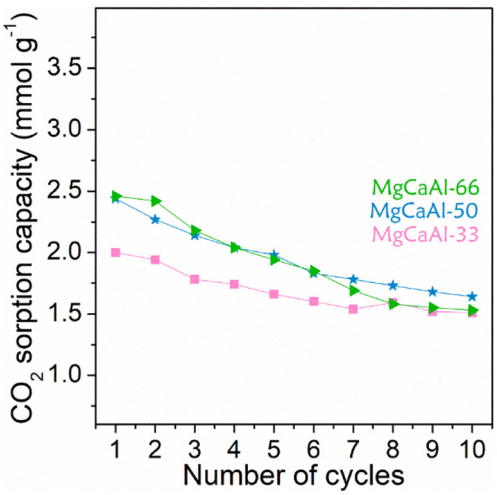

Fig. 9 CO_2 capture capacity (350 °C) of the calcined (800 °C) MgCaAl LDH compositions over 10 carbonation–decarbonation cycles.

Table 5 Comparison of the CO_2 sorption capacity of various MgAl-LDH materials reported in the literature

LDH	Sorption temperature (°C)	Sorption capacity (mmol g^{-1})	Ref.
Pristine LDH			
Mg_2Al-CO_3	200	0.90	29
Mg_2Al-CO_3 (SASOL)	400	0.32	34
Mg_3Al-CO_3	200	0.58	38
$Mg_2Al(OH)_6(CO_3)_{0.5}{\cdot}1.8H_2O$	200	1.06	Present
	400	0.61	work
Modified LDH			
Mg_2Al-CO_3 doped with 20% K_2CO_3	350	1.19	51
Mg_3Al-CO_3 doped with 20% K_2CO_3	400	0.83	34
$Mg_2(Al_{0.9}Ga_{0.1})$-CO_3	300	1.15	35
$Mg_2(Al_{0.9}Ga_{0.1})$-CO_3 with K_2CO_3	200	1.40	52
Mg_2CaAl-CO_3	350	1.28	36
$Mg_{1.3}Ca_{0.7}Al(OH)_6(CO_3)_{0.5}{\cdot}kH_2O$	350	1.87	Present
	400	3.09	work
$MgCaAl(OH)_6(CO_3)_{0.5}{\cdot}mH_2O$	350	2.39	
	400	4.55	
$Mg_{0.7}Ca_{1.3}Al(OH)_6(CO_3)_{0.5}{\cdot}nH_2O$	350	2.50	
	400	4.85	

while MgCaAl-50 and MgCaAl-66 display ~34% loss, as expected.

Calcined pristine MgAl LDH or Ca^{2+}-incorporated MgAl LDH with porous nanoplatelet morphology exhibit significantly enhanced sorption capacity compared to the related materials reported in the literature (Table 5).

4. Conclusions

Porous calcined MgAl LDH hexagonal nanoplatelets (surface area 115 m^2 g^{-1}) show a sorption capacity of 1.99 mmol g^{-1} at 30 °C, retaining 87% sorption capacity over 10 carbonation–decarbonation cycles. The calcined, calcium-modified MgAl LDH samples deliver enhanced capacity in the SEWGS temperature range of 200–400 °C. MgAl LDH with 66% calcium exhibits a stable CO_2 sorption capacity of 1 mmol g^{-1} over 10 cycles at 200 °C and 3.68 mmol g^{-1} at 400 °C with 85% capture efficiency retention after 10 cycles. Incorporation of Ca^{2+} in MgAl LDH results in the formation of uniformly dispersed CaO crystallites in the MMO formed on calcination. These CaO crystallites increase the surface-active Mg–O sites, leading to enhanced CO_2 sorption, and also render mechanical stability to the sorbent during thermal cycling.

Author contributions

BN: investigation and data curation; CN and MR: conceptualization, methodology, data curation, writing, review and editing. MR: funding acquisition and supervision.

Data availability

The data supporting this article have been included as part of the ESI.†

Conflicts of interest

There is no conflict of interest.

Acknowledgements

This work was funded by DST-SERB, New Delhi, India (EMR/2015/0001982). Support by DST-FIST funding (SR/FST/College-324/2016) for the procurement of a simultaneous thermal analyzer is acknowledged.

References

1 L. Santamaría, S. A. Korili and A. Gil, *Chem. Eng. J.*, 2023, **455**, 140551.
2 Z.-Z. Yang, J.-J. Wei, G.-M. Zeng, H.-Q. Zhang, X.-F. Tan, C. Ma, X.-C. Li, Z.-H. Li and C. Zhang, *Coord. Chem. Rev.*, 2019, **386**, 154.
3 X. Zhu, W. Xie, J. Wu, Y. Miao, C. Xiang, C. Chen, B. Ge, Z. Gan, F. Yang, M. Zhang, D. O'Hare, J. Li, T. Ge and R. Wang, *Chem. Soc. Rev.*, 2022, **51**, 6574.
4 J. Wang, L. Huang, R. Yang, Z. Zhang, J. Wu, Y. Gao, Q. Wang, D. O'Hare and Z. Zhong, *Energy Environ. Sci.*, 2014, **7**, 3478.
5 F. Kong, G. Rim, P. Priyadarshini, M. Song, M. J. Realff, R. P. Lively and C. W. Jones, *Sustainable Energy Fuels*, 2023, **7**, 4461.
6 X. Zhu, T. Ge, F. Yang, M. Lyu, C. Chen, D. O'Hare and R. Wang, *J. Mater. Chem. A*, 2020, **8**, 16421.
7 Z. Zhang, Z. P. Cano, D. Luo, H. Dou, A. Yu and Z. Chen, *J. Mater. Chem. A*, 2019, **7**, 20985.

8 S. Choi, J. H. Drese and C. W. Jones, *ChemSusChem*, 2009, **2**, 796.
9 X. Wang, T. He, J. Hu and M. Liu, *Environ. Sci.: Nano*, 2021, **8**, 890.
10 K. Sato and M. Hunger, *Commun. Chem.*, 2020, **3**, 91.
11 Y. Hu, Y. Guo, J. Sun, H. Li and W. Liu, *J. Mater. Chem. A*, 2019, **7**, 20103.
12 M. Krödel, A. Landuyt, P. M. Abdala and C. R. Müller, *ChemSusChem*, 2020, **13**, 6259.
13 F. Cavani, F. Trifiro and A. Vaccari, *Catal. Today*, 1991, **11**, 173.
14 M. Rajamathi, G. S. Thomas and P. V. Kamath, *J. Chem. Sci.*, 2001, **113**, 671.
15 C. Forano, U. Costantino, V. T. Prévot and C. Gueho, Layered double hydroxides (LDH), in *Handbook of Clay Science. Part A: Fundamentals, Developments in Clay Science*, ed. F. Bergaya and G. Lagaly, Elsevier, Amsterdam, 2nd edn, 2013, pp. 745–782.
16 A. I. Khan and D. O'Hare, *J. Mater. Chem.*, 2002, **12**, 3191.
17 G. R. Williams and D. O'Hare, *J. Mater. Chem.*, 2006, **16**, 3065.
18 S. Miyata, *Clays Clay Miner.*, 1983, **31**, 305.
19 Bhojaraj, J. Arulraj, M. R. Kolinjavadi and M. Rajamathi, *ACS Omega*, 2019, **4**, 20072.
20 Bhojaraj and M. Rajamathi, *ACS Omega*, 2023, **8**, 10185.
21 Bhojaraj, C. Nethravathi and M. Rajamathi, *Appl. Clay Sci.*, 2023, **243**, 107053.
22 L. Lei, A. I. Khan and D. O'Hare, *J. Solid State Chem.*, 2005, **178**, 3648.
23 S. P. Newman and W. Jones, *New J. Chem.*, 1998, **22**, 105.
24 Bhojaraj, C. Nethravathi and M. Rajamathi, *Dalton Trans.*, 2022, **51**, 9915.
25 J. H. Choy, S. Y. Kwak, J. S. Park, Y. J. Jeong and J. Portier, *J. Am. Chem. Soc.*, 1999, **121**, 1399.
26 M. León, E. Díaz, S. Bennici, A. Vega, S. Ordóñez and A. Auroux, *Ind. Eng. Chem. Res.*, 2010, **49**, 3663.
27 Q. Wang, H. H. Tay, Z. Guo, L. Chen, Y. Liu, J. Chang, Z. Zhong, J. Luo and A. Borgna, *Appl. Clay Sci.*, 2012, **55**, 18–26.
28 Q. Wang, Y. Gao, J. Luo, Z. Zhong, A. Borgna, Z. Guoc and D. O'Hare, *RSC Adv.*, 2013, **3**, 3414.
29 X. Kou, H. Guo, E. G. Ayele, S. Li, Y. Zhao, S. Wang and X. Ma, *Energy Fuels*, 2018, **32**, 5313.
30 L. Zhang, Y. Meng, G. Pan and S. Xia, *Inorg. Chem.*, 2020, **59**, 17722.
31 J. L. Gunjakar, I. Y. Kim and S.-J. Hwang, *Eur. J. Inorg. Chem.*, 2015, 1198–1202.
32 A. G. Gallastegui, D. Iruretagoyena, V. Gouvea, M. Mokhtar, A. M. Asiri, S. N. Basahel, S. A. Al-Thabaiti, A. O. Alyoubi, D. Chadwick and M. S. P. Shaffer, *Chem. Mater.*, 2012, **24**, 4531.
33 Q. Wang, H. H. Tay, D. J. W. Ng, L. Chen, Y. Liu, J. Chang, Z. Zhong, J. Luo and A. Borgna, *ChemSusChem*, 2010, **3**, 965.
34 X. Zhu, C. Chen, Q. Wang, Y. Shi, D. O'Hare and N. Cai, *Chem. Eng. J.*, 2019, **366**, 181.
35 C. Rocha, M. A. Soria and L. M. Madeira, *Sep. Purif. Technol.*, 2020, **235**, 116140.
36 X. P. Wang, J. J. Yu, J. Cheng, Z. P. Hao and Z. P. Xu, *Environ. Sci. Technol.*, 2008, **42**, 614.
37 N. D. Hutson and B. C. Attwood, *Adsorption*, 2008, **14**, 781.
38 Q. Wang, H. H. Tay, Z. Zhong, J. Luo and A. Borgna, *Energy Environ. Sci.*, 2012, **5**, 7526.
39 D. W. J. Leung, K. R. Laney, P. Kenyon, N. H. Rees, J.-C. Buffet, C. Chen and D. O'Hare, *Dalton Trans.*, 2024, **53**, 6200.
40 R. Rajamathi, Bhojaraj and C. Nethravathi, *ACS Appl. Nano Mater.*, 2021, **4**, 10969.
41 G. S. Thomas, M. Rajamathi and P. V. Kamath, *Clays Clay Miner.*, 2004, **52**, 693.
42 P. Bera, M. Rajamathi, M. S. Hegde and P. V. Kamath, *Bull. Mater. Sci.*, 2000, **23**, 141.
43 M. Bellotto, B. Rebours, O. Clause, J. Lynch, D. Bazin and E. Elkaïm, *J. Phys. Chem.*, 1996, **100**, 8535.
44 M. A. Aramendía, Y. Avilés, V. Borau, J. M. Luque, J. M. Marinas, J. R. Ruiz and F. J. Urbano, *J. Mater. Chem.*, 1999, **9**, 1603.
45 B. Rebours, J.-B. Caillerie and O. Clause, *J. Am. Chem. Soc.*, 1994, **116**, 1707.
46 F. Rey, V. Fornes and J. M. Rojo, *J. Chem. Soc., Faraday Trans.*, 1992, **88**, 2233.
47 Y. Gao, Z. Zhang, J. Wu, X. Yi, A. Zheng, A. Umar, D. O'Hare and Q. Wang, *J. Mater. Chem. A*, 2013, **1**, 12782.
48 N. N. A. H. Meis, J. H. Bitter and K. P. de Jong, *Ind. Eng. Chem. Res.*, 2010, **49**, 1229.
49 N. D. Hutson, *Chem. Mater.*, 2004, **16**, 4135.
50 H. A. Patel, J. Byun and C. T. Yavuz, *ChemSusChem*, 2017, **10**, 1303.
51 L. Sun, Y. Yang, H. Ni, D. Liu, Z. Sun, P. Li and J. Yu, *Ind. Eng. Chem. Res.*, 2020, **59**, 6043.
52 C. T. Yavuz, B. D. Shinall, A. V. Iretskii, M. G. White, T. Golden, M. Atilhan, P. C. Ford and G. D. Stucky, *Chem. Mater.*, 2009, **21**, 3473.